The Role of Leg Differentiation in Hexapedal Running

Sam Burden

Dr. Koditschek, Dr. Clark, and Joel Weingarten
SUNFEST REU 2006

ABSTRACT

Designing a robot that can autonomously traverse a variety of terrain types is difficult. For this reason, one may refer to nature for inspiration and produce robots that mimic biological organisms. EduBot is one such device, a hexapedal robot that resembles a cockroach. Building a robot that mimics a living creature offers numerous advantages, including design efficiency and locomotive stability. In addition, mathematical models that describe animal walking and running can be applied to the device, so an entire existing body of analysis can be used to characterize the robot's movement; this saves time and increases intuitive understanding. One such model, the spring-loaded inverted pendulum (or SLIP) model for animal running, has been successfully applied to EduBot's forward motion. However, like many animals, EduBot deviates from this model in that it exhibits a rolling motion about its forward axis. The goal of the current research is to describe this motion with a simple model and use the model to motivate modifications to the robot that will eliminate the roll. To characterize the roll, we measure the ground reaction forces from each of the robot's legs with a force plate and use a video-based motion capture system to record the robot's trajectory through space. We show that the maximum roll appears to decrease as the middle legs are made stiffer, which matches the prediction from the model.

Contents

1 INTRODUCTION

Calling upon nature to inform the design of a robotic device is a common technique in robotics; there exist numerous insect-like robots [1] [2], biologically-inspired implements like whiskers are common extensions for robotic sensing [3], and investigations into biological locomotion have potential applications to robotic movement [4].

The benefits of biomimesis in legged locomotion are numerous. First, a biological organism's gait is often efficient and passively stable. As a consequence, their artificial counterparts frequently exhibit these same qualities [5, 1]. Second, mathematical models created to describe a mimicked biological organism can be readily applied to the mimicking robotic device [6] [2]. Aside from simplifying analysis by permitting the use of established mathematical tools, this crossover provides a useful intuitive context for studying the robot.

One such biomimetic device is RHex, a cockroach-like hexapedal robot [1]; it is fast, highly mobile, and relatively stable [7]. A model from biological investigations which has found fruitful application to RHex is the spring-loaded inverted pendulum (SLIP) model for running and hopping [8]. In the SLIP model, the organism in question is abstracted as having only a single spring-loaded leg. This leg contacts the ground at one end and is attached to the body's mass at the other. The SLIP model has been successfully applied to a wide variety of animals [9], as well as RHex [6]. Applying the SLIP model to RHex's motion is useful for two reasons. First, it provides an underlying intuition for why the robot moves so efficiently and so stably. Second, it provides a simple enough *template* for the robot's motion that actual analysis can be performed on the stability [5, 10], providing a mathematical explanation for the observed robustness of the robot's gait. We work here with a smaller version of RHex called EduBot whose design and movement is similar to its predecessor. We are thus motivated to seek similarly simple and descriptive models for other aspects of EduBot's motion with the dual purpose of understanding the basic mechanical properties of the robot intuitively and of providing a rigorous justification for its design.

In particular, EduBot exhibits a seemingly periodic and stable *rolling motion* about the forward axis. It is unclear what, exactly, is causing this lateral roll. More importantly, it is unclear how this roll affects the overall forward motion. It is possible the rolling contributes to stability or efficiency, but it is also perfectly possible that the rolling motion adversely affects both. We present here a simple model for the roll and use the model to inform a modification to the robot's hardware intended to eliminate the roll.

Various techniques have been developed for modeling and analyzing equilibrium gaits. We take as a simple and canonical example the passive walker [11] [12] and attempt to perform a similar sort of analysis using techniques from the field [13] [14]. Since we find that our model's dynamics cannot be integrated directly, we are forced to pose the problem in less direct terms in an attempt to prove gait properties [5, 10] [15].

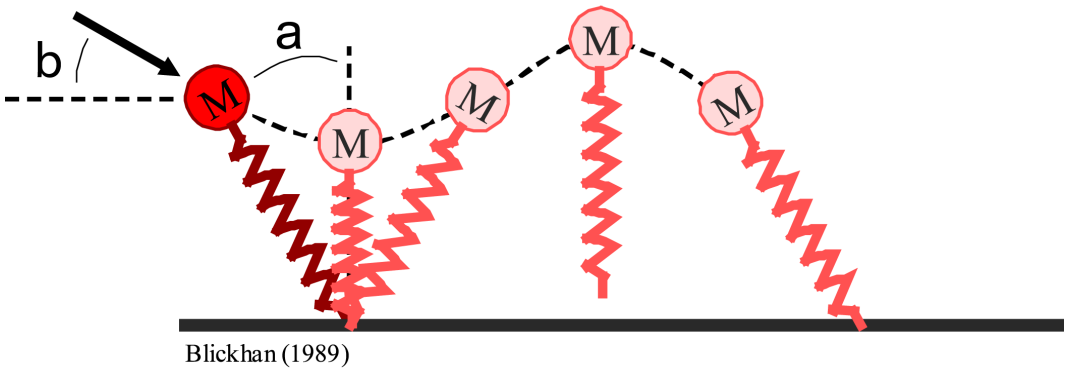

Figure 1: Example trajectory for the Spring-Loaded Inverted Pendulum Model for animal running.

1.1 OVERVIEW

We begin with a discussion of the SLIP model for animal running, which is meant to introduce the reader to the type of modeling problems that have been studied before. We then present some data recorded with EduBot and note some of the salient characteristics of the robot's gait. Then we develop a conservative model for EduBot's roll and discuss some analytical and numerical results. Finally, we describe a damped model for the robot's rolling motion and present numerical results that suggest a certain physical modification to EduBot will eliminate the roll and present the results of the physical modification.

2 BACKGROUND

2.1 SPRING-LOADED INVERTED PENDULUM MODEL

We were motivated in the design and analysis of our rolling model by the success of the simple Spring-Loaded Inverted Pendulum (or SLIP) hybrid dynamical model for animal running. SLIP has been applied to a variety of animals [9], and even artificial creatures [2] [6], and analysis of the model has yielded insight into the fundamental nature of RHex and EduBot's stability [5, 10].

The SLIP model consists of a single point mass attached to one end of a spring; see Figure 1. This mass M is projected toward the ground with velocity $\vec{v} = (v\cos\beta, v\sin\beta)$ while the spring is fixed at an angle α from the y-axis. When the spring strikes the ground, the point of contact is fixed. The spring then compresses, pivots, and uncompresses. When the spring reaches its nominal length l_0, it leaves the ground and the mass-spring system experiences a flight phase.

During flight, the system's dynamics are transparent. Namely,

$$x(t) = x_0 + \dot{x}_0 t, \quad y(t) = y_0 + \dot{y}_0 - \frac{1}{2}gt^2, \tag{1}$$

where $(x_0, \dot{x}_0, y_0, \dot{y}_0)$ represents the system's state at liftoff. During stance, the system can be described via its Lagrangian $L = T - V$ in terms of the mass's position (x, y); specifically,

$$T = \frac{1}{2}M(\dot{x}^2 + \dot{y}^2),\ V = gMy + \frac{1}{2}(l_0 - \sqrt{x^2 + y^2})^2, \tag{2}$$

which leads to the equations of motion for the mass during stance,

$$\ddot{x} = x\frac{k}{m}(\frac{l_0}{\sqrt{x^2 + y^2}} - 1),\ \ddot{y} = y\frac{k}{m}(\frac{l_0}{\sqrt{x^2 + y^2}} - 1) - g. \tag{3}$$

These equations cannot be solved analytically as they stand. Koditschek [10] has shown that if gravity is neglected during stance (corresponding physically to the use of relatively stiff springs), then a closed-form solution exists, up to the evaluation of a (difficult) integral.

When working with the conservative SLIP model, one typically only considers equilibrium trajectories, which are those with a constant forward velocity during consecutive flight phases.

3 CONSERVATIVE MODEL FOR ROLL

Noting the success the SLIP model has had in describing the robot's sagittal-plane motion and the success researchers have had in producing analytical results about the stability of the model, we attempt to apply similar methods of analysis to the robot's roll about its forward axis.

It seems possible, if not plausible, that this rolling motion is due primarily to an imbalance in weight distribution during running. Specifically, EduBot utilizes an *alternating tripod gait* when running: the two front legs on one side of the body are in contact with the ground while only the middle leg touches down on the other. Since the legs are compliant, this imbalance likely compresses one more than the other, resulting in a lateral rolling motion.

To model this behavior, we imagine two massless linear springs attached to either side of a rod of mass M, moment of inertia J, and width $2w$ (see Figure 2); for the majority of our experiments, we assume that mass is distributed evenly throughout EduBot . Assuming the robot's legs are very similar due to a fairly precise construction process (supported by preliminary data), the springs in the model have identical nominal lengths, l_0. But as there are two legs in contact with the ground on one side of the robot while only one on the other, the spring constants k_1 and k_2 are in general unequal.

3.1 PRELIMINARY JUSTIFICATION

As EduBot runs, it takes full advantage of its rigid body's six degrees of freedom: the robot rolls, twists, pitches, slides, jumps, and runs. To simplify the analysis, we proceed by assuming that the jumping and rolling motions are decoupled from the rest and analyze them exclusively. This is a strict assumption, since the full-body dynamics certainly have an effect on the rolling motion.

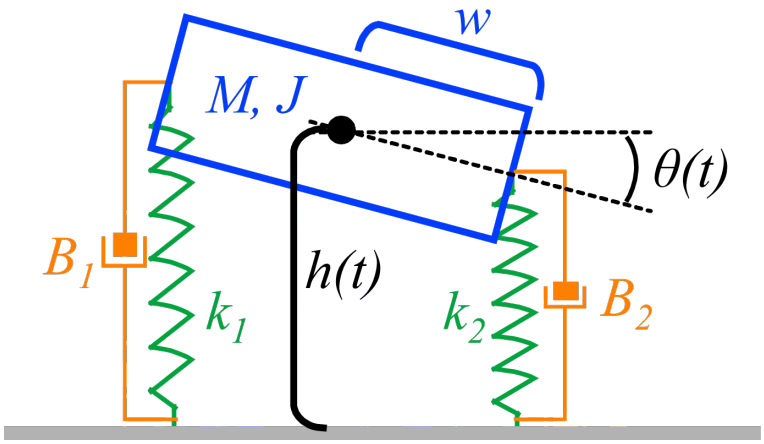

Figure 2: Simple spring-mass model for EduBot's rolling motion. In general, $k_1 \neq k_2$. We set $B_1 = B_2 = 0$ when we wish to study a conservative model.

When running at equilibrium, EduBot follows roughly periodic rolling and bounding trajectories. Figure 3 shows such a trajectory (see Appendix D) next to one obtained from the conservative model discussed here. There are a few distinctive qualitative behaviors to note about EduBot's trajectory: first, the center of mass oscillates up and down with a fixed frequency; second, the robot's roll has a distinct, periodic form that the model roughly captures.

The previous discussion does not completely specify the model, as there are some constraints we must impose on the dynamics. First, we fix the center of mass of the rod to only move in the vertical direction (as if fixed on a rail), and allow the 'feet' of the springs to slide frictionlessly across the ground. This removes one degree of freedom from the system, and is a reasonable simplification, since the robot doesn't move much laterally on average. Second, it doesn't make any sense to allow the rod to flip around—if it rotates beyond $\pm\frac{\pi}{2}$, the model is nonphysical. We get around this by simply not allowing simulations or analysis to proceed into that region of state space. Third, we allow the springy legs to come off the ground, and thus for the rod to attain a *flight phase*. When one or both legs are off the ground, the dynamics should alter accordingly. This puts the model into the analytically challenging realm of *hybrid dynamics* [13], but is necessary to capture the dynamics we are interested in.

Now we have an analytical choice to make about the set of coordinates for our two degree-of-freedom system. Two obvious choices are to record the two spring lengths (x_1, x_2) or the height of the center of mass of the rod and the rod's rotation (h, θ); we found the equations in (h, θ) space to be more amenable.

Note that $\mathbf{X} = \{(x_1, x_2) \in \mathbb{R} \times \mathbb{R}\}$ is a linear vector space, whereas $\mathbf{\Theta} = \{(h, \theta) \in \mathbb{R} \times e^{i\mathbb{R}}\}$ isn't. The transformation $\mathbf{X} \leftrightarrow \mathbf{\Theta}$ is therefore nonlinear. In fact, a simple computation yields (with θ increasing counterclockwise)

$$h = \frac{x_1 + x_2}{2}, \ \sin\theta = \frac{x_2 - x_1}{2w}, \tag{4}$$

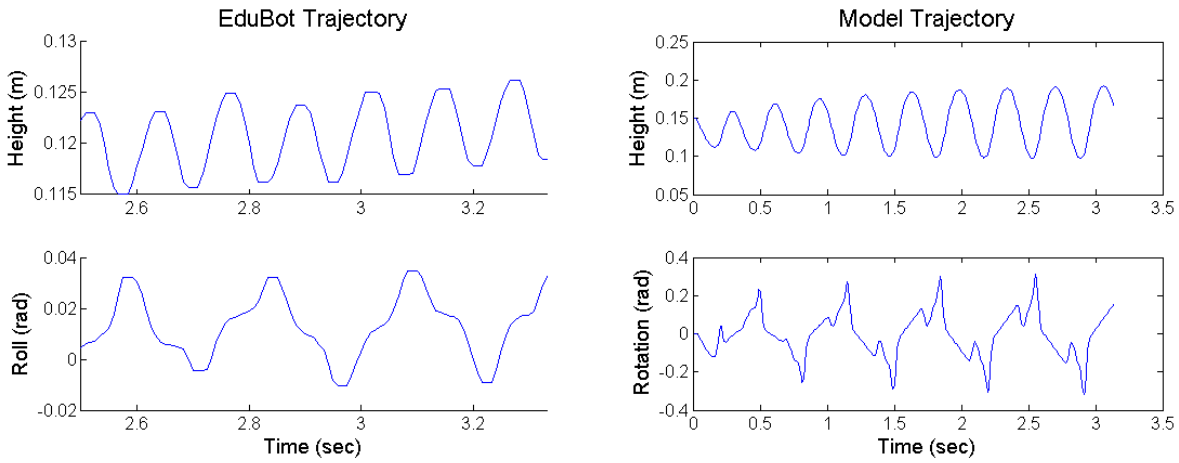

Figure 3: Rolling and height trajectories from EduBot data and from simulation; experimental data was filtered (see Appendix D). There is significant deviation in both coordinates, but the model qualitatively captures some of the distinctive behavior exhibited by the robot.

a decidedly nonlinear transformation in θ.

Now that we have settled on a coordinate system and have determined all the model's parameters, we can write down and analyze the equations of motion for the rod. We choose to find these equations using the *Lagrangian* $L = T - V$, where T is the kinetic energy of the system and V the potential in the generalized coordinates. (Use of the Lagrangian is not necessary; the same result follows using Newton's laws directly.) Our equations of motion then become

$$\frac{\partial L}{\partial h} - \frac{\partial}{\partial t}\frac{\partial L}{\partial \dot{h}} = 0, \;\; \frac{\partial L}{\partial \theta} - \frac{\partial}{\partial t}\frac{\partial L}{\partial \dot{\theta}} = 0. \tag{5}$$

Analysis of the model during stance yields

$$T = \frac{1}{2}M\dot{h}^2 + \frac{1}{2}J\dot{\theta}^2, \;\; V = Mgh + \frac{1}{2}k_1(l_0 - (h - w\sin\theta))^2 + \frac{1}{2}k_2(l_0 - (h + w\sin\theta))^2. \tag{6}$$

Solving the equations of motion for $\ddot{h}$ and $\ddot{\theta}$, we find

$$\begin{aligned} \ddot{h} &= \tfrac{1}{M}\left(-gM + w\sin\theta(k_1 - k_2) - (h - l_0)(k_1 + k_2)\right), \\ \ddot{\theta} &= \tfrac{1}{J}\left(w\cos\theta\left((h - l_0)(k_1 - k_2) - w\sin\theta(k_1 + k_2)\right)\right). \end{aligned} \tag{7}$$

3.2 STANCE EQUILIBRIUM

We now turn to the task of finding stationary points of the system defined by eq. 7 when the robot never leaves the ground; specifically, we're interested in fixing $\dot{\theta} \equiv 0$. Intuitively, it seems there can be only a few, and it seems unlikely that there would be any dynamic solutions (i.e. solutions with $\dot{h}(t) \neq 0$ for some t). We therefore seek to back up this intuition with precise mathematical reasoning.

STATIC SOLUTION The static solution that ensures $\dot{\theta} \equiv 0$ can be found by applying static analysis to the system. When stationary, the springs will have to support the entire weight of the block, so $k_1\Delta x_1 + k_2\Delta x_2 = Mg$. An additional equation relating the Δx's comes from observing that the sum of torques acting on the block must be zero at equilibrium, and therefore $k_1\Delta x_1 cos\theta - k_2\Delta x_2 cos\theta = 0$. Combining these two equations (and excluding the case[1] $\theta = \pm\frac{\pi}{2}$), we see that $\Delta x_i = \frac{gM}{2k_i}, i = 1, 2$. Using eq. 4, the resulting equilibrium condition is

$$h_0 = l_0 - \frac{gM}{4}\left(\frac{1}{k_1} + \frac{1}{k_2}\right),\ \dot{h}_0 = 0,\ \sin\theta_0 = \frac{gM}{4w}\left(\frac{1}{k_1} - \frac{1}{k_2}\right),\ \dot{\theta}_0 = 0. \tag{8}$$

Substituting these initial values into eq. 7 yields $\ddot{h} = \ddot{\theta} = 0$, so the system is at static equilibrium for all time. Note, conveniently, that if $k_1 \neq k_2$, these equations imply

$$h_0 = l_0 - \frac{gM}{2},\ \dot{h}_0 = 0,\ \theta_0 = 0,\ \dot{\theta}_0 = 0, \tag{9}$$

exactly the static equilibrium condition expected for a simple spring-mass system.

DYNAMIC SOLUTION At this point, the question arises: are there any dynamic solutions that ensure $\dot{\theta} \equiv 0$? Using physical intuition, it would seem that if one found a point where the sum of torques was zero, raising or lowering the mass would cause a torque imbalance to appear, thus giving the body a nonzero angular velocity. This argument is nearly rigorous, and can probably be made quite precise, but we prefer instead to turn to the equations of motion to find a mathematical justification for this intuitive explanation.

From eq. 7, we can solve for h in terms of $\ddot{h}$ and $\sin\theta$:

$$h = \frac{1}{k_1 + k_2}\left[-gM - \ddot{h}M + k_1(H + w\sin\theta) + k_2(H - w\sin\theta)\right]. \tag{10}$$

Also from eq. 7, assuming $\ddot{\theta} \equiv 0$ (required for $\dot{\theta} \equiv 0$) yields

$$\sin\theta = \frac{(k_1 - k_2)(h - l_0)}{w(k_1 + k_2)}. \tag{11}$$

Now, substituting eq. 10 into eq. 11,

$$\sin\theta = \frac{M(g + \ddot{h})}{4w}\left(\frac{1}{k_1} - \frac{1}{k_2}\right). \tag{12}$$

Note that if $\ddot{h} \equiv 0$, this is exactly the case we found for static equilibrium. If $\ddot{h}(t_0) = \eta \neq 0$, then $\ddot{h} \equiv \eta$, because otherwise θ changes in time, which means $\dot{\theta} \neq 0$ at some time. But it would require an infinite amount of energy to ensure $\ddot{h} \equiv \eta \neq 0$, so this case is nonphysical. Therefore *there does not exist* a system trajectory that sets $\dot{\theta} \equiv 0, \dot{h}(t) \neq 0$.

[1] This is physically justified, since we don't intend to analyze the case where the robot rolls onto its side.

3.3 HYBRID DYNAMICAL EQUILIBRIUM

Now that we have shown no dynamic stance equilibria can exist, we turn our attention to the generally more difficult realm of *hybrid dynamical systems*, where the governing equations of motion are allowed to change as functions of state. We use the formalism given by Guckenheimer [13], which treats a hybrid system as a collection of 4-tuples $(F_\alpha, V_\alpha, \mathcal{H}_\alpha^\beta, \mathcal{T}_\alpha^\beta)$ indexed by $\alpha, \beta \in \mathbf{D}$, where $\mathbf{D}$ is a set of dynamical regimes. In this framework, $F_\alpha : \mathbb{R}^5 \to \mathbb{R}^4$ governs how the system progresses through state space in a certain regime α and can be written implicitly as the solution to a system of differential equations, $V_\alpha \subset R^4$ represents the region of state space reachable in α, $\mathcal{H}_\alpha^\beta : \mathbb{R}^4 \to \mathbb{R}$ are *threshold functions* that go to zero when the system transitions from regime α to β, and $\mathcal{T}_\alpha^\beta : \mathbb{R}^4 \to \mathbb{R}^4$ are *transition functions* that describe how to transition between V_α and V_β. In the model presented here, there are four regimes: flight, left leg stance, right leg stance, and full stance, denoted by $\mathcal{F}$, $\mathcal{L}$, $\mathcal{R}$, and $\mathcal{S}$, respectively.

3.3.1 ANALYTICAL METHODS

AN APPROXIMATION To approach the problem of finding equilibrium gaits analytically, we first make an approximation. Since the robot tilts less than 15^o in the regime we are interested in, we make a small-angle approximation, $\sin\theta \mapsto \theta$. This has the effect of reducing our system to a fourth-order system of linear differential equations, which vastly simplifies the analysis.

EQUATIONS OF MOTION Our first step is to describe the equations of motion that govern each regime, the F_α's. During flight, we can solve explicitly for $z(t) = (h(t), \dot{h}(t), \theta(t), \dot{\theta}(t))$. Indeed,

$$F_{\mathcal{F}}(t, (h, \dot{h}, \theta, \dot{\theta})) = \begin{bmatrix} h_k + \dot{h}_k t - \frac{1}{2} g t^2 \\ 0 \\ \theta_k + \dot{\theta}_k t \\ 0 \end{bmatrix}, \tag{13}$$

where $(h_k, \dot{h}_k, \theta_k, \dot{\theta}_k)$ is the state of the system at the k^{th} liftoff event.

During stance, we can put the equations in the form $\dot{z}(t) = Az + b$, where A is (4×4) and b is (4×1). During full stance,

$$\begin{bmatrix} \dot{h}(t) \\ \ddot{h}(t) \\ \dot{\theta}(t) \\ \ddot{\theta}(t) \end{bmatrix}_{\mathcal{S}} = \begin{bmatrix} 0 & 1 & 0 & 0 \\ \frac{1}{M}(k_1 + k_2) & 0 & -\frac{w}{M}(k_1 - k_2) & 0 \\ 0 & 0 & 0 & 1 \\ \frac{w}{J}(k_1 - k_2) & 0 & -\frac{w^2}{J}(k_1 + k_2) & 0 \end{bmatrix} \begin{bmatrix} h(t) \\ \dot{h}(t) \\ \theta(t) \\ \dot{\theta}(t) \end{bmatrix}_{\mathcal{S}} + \begin{bmatrix} 0 \\ H(k_1 + k_2) - gM \\ 0 \\ wH(k_1 - k_2) \end{bmatrix}. \tag{14}$$

To compute the partial stance equations of motion, simply omit one of the spring constants in eq. 14: remove k_1 to get the equations for $\mathcal{R}$; remove k_2 to get the equations for $\mathcal{L}$. To be explicit,

$$\begin{bmatrix} \dot{h}(t) \\ \ddot{h}(t) \\ \dot{\theta}(t) \\ \ddot{\theta}(t) \end{bmatrix}_{\mathcal{L}} = \begin{bmatrix} 0 & 1 & 0 & 0 \\ \frac{1}{M}k_1 & 0 & -\frac{w}{M}k_1 & 0 \\ 0 & 0 & 0 & 1 \\ \frac{w}{J}k_1 & 0 & -\frac{w^2}{J}k_1 & 0 \end{bmatrix} \begin{bmatrix} h(t) \\ \dot{h}(t) \\ \theta(t) \\ \dot{\theta}(t) \end{bmatrix}_{\mathcal{L}} + \begin{bmatrix} 0 \\ Hk_1 - gM \\ 0 \\ wHk_1 \end{bmatrix}, \tag{15}$$

$$\begin{bmatrix} \dot{h}(t) \\ \ddot{h}(t) \\ \dot{\theta}(t) \\ \ddot{\theta}(t) \end{bmatrix}_{\mathcal{R}} = \begin{bmatrix} 0 & 1 & 0 & 0 \\ \frac{1}{M}k_2 & 0 & \frac{w}{M}k_2 & 0 \\ 0 & 0 & 0 & 1 \\ -\frac{w}{J}k_2 & 0 & -\frac{w^2}{J}k_2 & 0 \end{bmatrix} \begin{bmatrix} h(t) \\ \dot{h}(t) \\ \theta(t) \\ \dot{\theta}(t) \end{bmatrix}_{\mathcal{R}} + \begin{bmatrix} 0 \\ Hk_2 - gM \\ 0 \\ -wHk_2 \end{bmatrix}. \tag{16}$$

THRESHOLD FUNCTIONS A threshold function is denoted $\mathcal{H}_\alpha^\beta(z)$, where α is the starting dynamical regime and β the ending one; a transition occurs when $\mathcal{H}_\alpha^\beta(z) = 0$. Each $\mathcal{H}$ is accompanied by a corresponding *transition function* $\mathcal{T}_\alpha^\beta(z)$ that specifies how to map points in the space associated with α to the one associated with β, although in all cases presented here, $\mathcal{T}_\alpha^\beta(z)$ is the identity function.

It is somewhat easier to think about the threshold equations using a different set of coordinates. Specifically, we will rely on the substitutions

$$x_1 = l_0 - (h - w\theta),\ x_2 = l_0 - (h + w\theta), \tag{17}$$

$$\dot{x}_1 = -\dot{h} + w\dot{\theta},\ \dot{x}_2 = -\dot{h} - w\dot{\theta}. \tag{18}$$

When in flight,

$$\begin{aligned} \mathcal{H}_{\mathcal{F}}^{\mathcal{S}}(z) &= (l_0 - h)^2 + (\theta)^2, -\dot{h} - w|\dot{\theta}| \leq 0, \\ \mathcal{H}_{\mathcal{F}}^{\mathcal{L}}(z) &= (x_1)^2,\ \dot{x}_1 \leq 0,\ \theta > 0, \\ \mathcal{H}_{\mathcal{F}}^{\mathcal{R}}(z) &= (x_2)^2,\ \dot{x}_2 \leq 0,\ \theta < 0. \end{aligned} \tag{19}$$

When in stance,

$$\begin{aligned} \mathcal{H}_{\mathcal{S}}^{\mathcal{F}}(z) &= (l_0 - h)^2 + (\theta)^2, -\dot{h} - w|\dot{\theta}| > 0, \\ \mathcal{H}_{\mathcal{S}}^{\mathcal{L}}(z) &= (x_1)^2,\ \dot{x}_1 > 0,\ \theta < 0, \\ \mathcal{H}_{\mathcal{S}}^{\mathcal{R}}(z) &= (x_2)^2,\ \dot{x}_2 > 0,\ \theta > 0. \end{aligned} \tag{20}$$

When in left stance,

$$\begin{aligned} \mathcal{H}_{\mathcal{L}}^{\mathcal{R}}(z) &= (l_0 - h)^2 + (\theta)^2,\ \dot{x}_1 > 0,\ \dot{x}_2 < 0, \\ \mathcal{H}_{\mathcal{L}}^{\mathcal{F}}(z) &= (x_1)^2,\ \dot{x}_1 > 0,\ \dot{x}_2 > 0, \\ \mathcal{H}_{\mathcal{L}}^{\mathcal{S}}(z) &= (x_2)^2,\ \dot{x}_1 < 0,\ \dot{x}_2 < 0. \end{aligned} \tag{21}$$

When in right stance,

$$\begin{aligned} \mathcal{H}_{\mathcal{R}}^{\mathcal{L}}(z) &= (l_0 - h)^2 + (\theta)^2,\ \dot{x}_1 < 0,\ \dot{x}_2 > 0, \\ \mathcal{H}_{\mathcal{R}}^{\mathcal{F}}(z) &= (x_1)^2,\ \dot{x}_1 > 0,\ \dot{x}_2 > 0, \\ \mathcal{H}_{\mathcal{R}}^{\mathcal{S}}(z) &= (x_2)^2,\ \dot{x}_1 < 0,\ \dot{x}_2 < 0. \end{aligned} \tag{22}$$

POINCARÉ MAP The definition of an equilibrium gait in the hybrid dynamical case departs significantly from the definition given in Section 3.2. Here we require that since the spring constants are exchanged during flight (to model EduBot's *alternating tripod gait*[2]), each touchdown state $(h_k, \dot{h}_k, \theta_k, \dot{\theta}_k)$ must be the mirror image of the previous touchdown state $(h_{k-1}, \dot{h}_{k-1}, \theta_{k-1}, \dot{\theta}_{k-1})$; i.e.

$$(h_k, \dot{h_k}, \theta_k, \dot{\theta}_k) = (h_{k-1}, \dot{h}_{k-1}, -\theta_{k-1}, -\dot{\theta}_{k-1}). \tag{23}$$

Note that h_k and θ_k, the height and rotation at the k^{th} touchdown, are related:

$$l_0 = h - w \sin|\theta|\,, \tag{24}$$

Thus, we can define a *Poincaré section* Σ (see Appendix A),

$$\Sigma = \{(h, \dot{h}, \theta, \dot{\theta}) \in \mathbb{R}^4 \mid l_0 = h - w \sin|\theta|\} = \{(h_k, \dot{h}_k, \theta_k, \dot{\theta}_k)\}, \tag{25}$$

Note that the restriction $l_0 = h - w \sin|\theta|$ implies that Σ is a three-dimensional hypersurface in the four-dimensional state space.

Technically speaking, Σ is only a Poincaré section if it is *transverse* to the system trajectories that we are interested in. Formally, this means if the system touches down at time t_k, $k > 0$, $\phi_{t_k}(x_0) \cdot n_\Sigma(x_k) \neq 0$, where $x_k = (h(t_k), \dot{h(t_k)}, \theta(t_k), \dot{\theta}(t_k)) \in \Sigma$ is the state of the system at touchdown, $n_\Sigma(x_k)$ is the normal vector to Σ at x_k, and $\phi_t(x_0)$ is a system trajectory that passes through Σ. Intuitively, this means the trajectory cannot travel along Σ, i.e., trajectories intersect Σ at discrete points.

In the physical system this condition is always met. To see this, look at a trajectory $\phi_t(x_0)$ that intersects Σ. Suppose at time t_k the body just contacts the ground, yet $\dot{h}(t_k) = \dot{\theta}(t_k) = 0$ (otherwise at time $t_k + \epsilon$, $0 < \epsilon \ll 1$, the system has passed through Σ). Now, considering a point on Σ,

$$l_0 = h(t_k) - w \sin|\theta(t_k)|\,. \tag{26}$$

Substituting this into the equations of motion for the system (eq. 7) we find that if $\theta = 0$, $\ddot{h} \neq 0$ and the trajectory passes through Σ. If $\theta \neq 0$, then $M\ddot{h} = -gM \pm 2k_i w \sin|\theta|$, where $i \in \{1, 2\}$. Now $\ddot{h} = 0 \iff \sin|\theta| = \frac{gM}{2k_i w}$. For the range of parameters we use in our model, this angle lies in the right half-plane, so it is not *a priori* an impossible choice. The choice for $\sin|\theta|$ implies $J\ddot{\theta} = -w \cos|\theta|\,(\pm gM)$, which, given that the robot doesn't land on its side, is nonzero. Thus all system trajectories we are interested in are transverse to Σ, so Σ is a Poincaré section.

With the formal definition of what we mean by an equilibria in the hybrid dynamical system, we would like to proceed by finding the equilibria analytically and comment on their stability. Unfortunately, this is such a difficult task that we have made little progress. To use the Poincaré section, we would need to find an explicit formula for the corresponding Poincaré map, which

[2]The front and rear legs on one side of EduBot are synchronized with the middle leg on the other. In a gait with a flight phase, this means only three legs are in contact with the ground during stance.

we have not yet been able to do. To find the equilibria by some other insight may be possible, but we have yet to discover the method. Thus, we resort to numerical analysis to investigate the system's equilibria.

3.3.2 NUMERICAL METHODS

VECTOR FIELD We start the system simulation (see Appendix C) from a mesh of initial conditions $x_0^{i,j} \in \Sigma$ and record the next point $x_1^{i,j}$ in the trajectory that intersects Σ. We then make a vector field plot of this data, connecting the initial condition with the final condition[3] by a directed line segment (head toward the final condition). $\dot{\theta}_k$ is plotted along the x-axis and θ_k along the y-axis, and since $\dot{h}_k$ is determined up to a sign difference by $\dot{\theta}_k$ (by conservation of energy), it determines the color of the vector. Since h_k is determined by θ_k by the threshold equation, it is not contained in the plot.

Unfortunately, due to the unstable nature of the system, x_1 generally lands very far from x_0, so these plots initially appear as a mess of intersecting lines. To make the plots useful, they show vectors at $1/10^{th}$ or $1/20^{th}$ their original magnitude; without carefully noting this fact, the data is distorted. For instance, the scaled-down plots give the impression that the flow field has stable equilibria, which is almost certainly false.

The point of generating these plots is to gain an intuitive understanding of how the system progresses from one set of initial conditions to another. One important goal is to identify equilibrium gaits and determine (roughly in this case) their stability. To identify a fixed point, we iteratively produce a vector field plot over a given range of parameters, choose the smallest vector in the plot, and shrink the field range around that point. After ten iterations, we typically achieve estimates on the fixed point good to about 1%.

RESULTS Figure 4 contains a plot of the conservative vector field with the period-one fixed point highlighted and enhanced. By narrowing our vision around the approximate fixed point and remembering that the vectors in the plots are scaled by a factor of 1/20, we begin to see behavior that suggests an unstable equilibrium. Namely, the fixed point rests on a very narrow well, and any deviation from the point is amplified by successive strides.

Even if it turns out that the fixed point is *locally* stable with a small basin of attraction, we find this physically irrelevant; EduBot clearly exhibits a high degree of stability, so we have no interest in discussing infinitesimally-attracting equilibrium gaits. For this reason, we turn toward the investigation of a damped version of the model discussed here to describe EduBot's rolling motion.

[3]We actually plot the final condition *after applying the map* $(\theta, \dot{\theta}) \mapsto -(\theta, \dot{\theta})$; this takes into account the fact that the leg spring constants are exchanged during flight, and means shorter vectors correspond to more symmetric gaits.

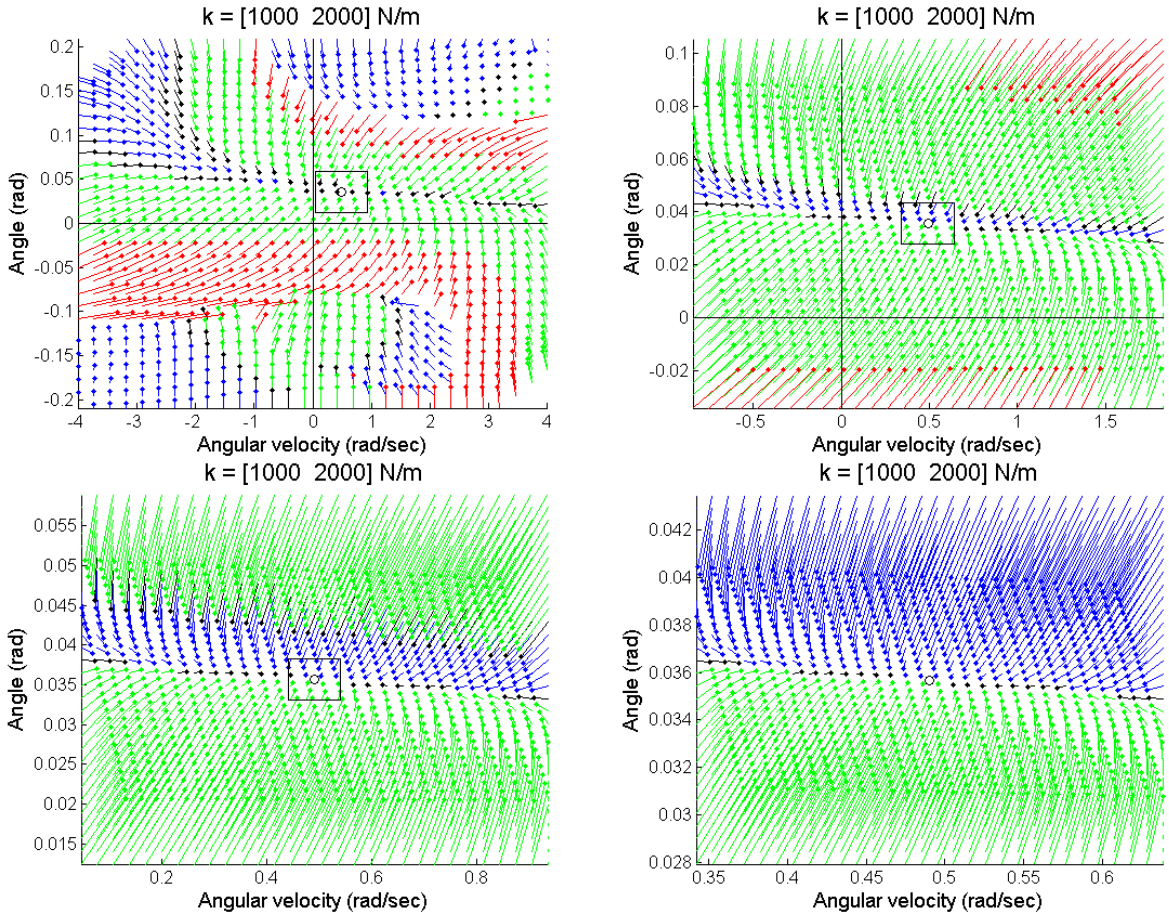

Figure 4: Conservative vector field; unstable period-one fixed point highlighted. Vectors scaled by $1/20^{th}$ for clarity.

4 DAMPED MODEL FOR ROLL

Given substantial numerical evidence that the period-one equilibrium gaits in the conservative model for EduBot's roll are (at the very least) not significant attractors, we proceed to add damping to the model with the hope that the attractive basins surrounding fixed points will enlarge considerably, making stable equilibrium gaits.

Note that if we were to solely add viscous damping to the model in Section 3, our simulations would become degenerate very quickly. Without a corresponding method to add energy to the system, there would be precisely one (very stable!) globally attracting equilibrium gait with infinite (or zero) stride period: the static gait described by

$$(h, \dot{h}, \theta, \dot{\theta}) \equiv (l_0 - \frac{gM}{4}\left(\frac{1}{k_1} + \frac{1}{k_2}\right),\ 0,\ sin^{-1}\left(\frac{gM}{4w}\left(\frac{1}{k_1} - \frac{1}{k_2}\right)\right),\ 0). \tag{27}$$

Thus, we simultaneously add an energy-addition scheme to the conservative model.

ENERGY ADDITION We add energy to the system in a similar manner to Koditschek and Buehler [16]: when a spring reaches maximum compression in the model, we temporarily increase its spring constant, thus increasing the energy stored in the spring. When a spring leaves the ground, its spring constant is reset. Maximum compression is detected when a leg's velocity goes to zero,

$$-\dot{h} \pm w\dot{\theta} = 0, \tag{28}$$

where the $\pm$ is determined by which leg is being considered. At that instant, the spring constant k_i is multiplied by an increase factor $\gamma > 1$. When the leg leaves the ground, the spring constant is reset to its initial value.

This energy addition scheme was chosen because it is easy to implement and can facilitate analysis better than many other methods. However, it is a poor model for the physical system and could be a source of qualitative disagreement between experimental and simulation results; we do not investigate the affect of changing the energy addition scheme here.

Figure 5 contains a plot of the damped vector field with one of the period-one fixed points highlighted and enhanced. Note that vector scaling in this figure is half what it was for the conservative system plots. There is actually a second fixed point, which can be seen in the lower half-plane of the upper-left plot; it corresponds to a gait which lands first on the stiff leg. The period-one equilibrium gait we found for the conservative system lands first on the soft leg, so we consider this the *dominant* equilibrium gait, and choose to highlight it in Figure 5. The second fixed point will be referred to as the *suppressed* equilibrium gait.

4.1 ELIMINATING ROLL

SPRING CONSTANTS When we constructed the current model, we assumed that the difference in spring constants drives the rolling motion observed in EduBot, and that letting

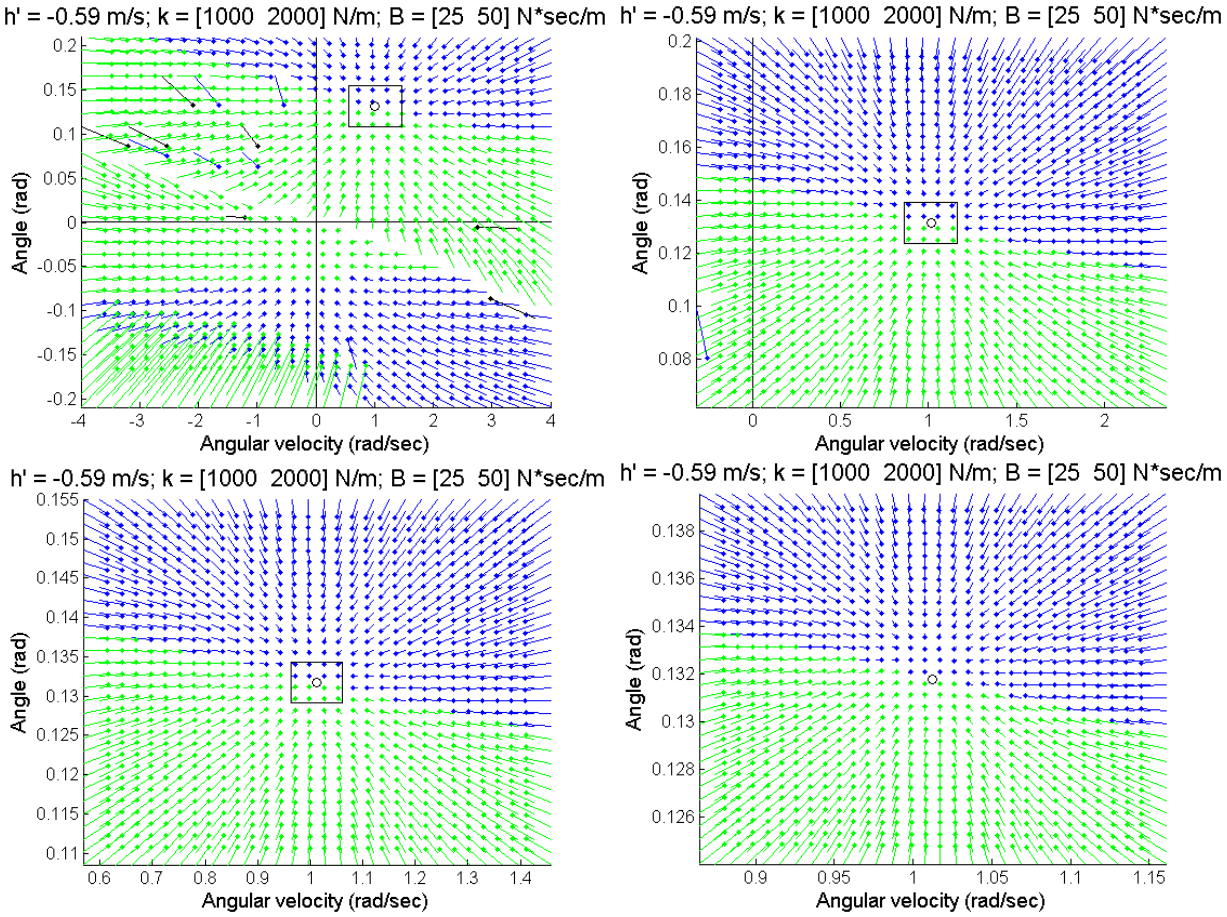

Figure 5: Damped vector field; dominant stable period-one fixed point highlighted. Vectors scaled by $1/10^{th}$ for clarity. Though θ determines h at touchdown as in the conservative model, energy dissipation implies $\dot{h}$ isn't determined by $\dot{\theta}$. Thus, these plots show a particular $\dot{h}$-slice; $\dot{h} = -0.59$ m/sec.

$k_1 \to k_2$ would likely eliminate the roll[4]. However, we were not sure how the equilibrium gaits would move toward the origin and what would happen to the gaits' stability as $k_1 \to k_2$. To study the progression of the equilibrium gaits toward the origin, we first compute fixed points of the Poincaré map $\mathcal{P}$ associated with Σ to desired error tolerances, then numerically compute the *Jacobian* of $\mathcal{P}$, $\frac{\partial \mathcal{P}}{\partial(h,\dot{h},\theta,\dot{\theta})}$, to determine how the stability of the gaits changes.

EQUILIBRIUM GAITS Based on physical intuition and qualitative numerical evidence, we proceed by assuming that equilibrium gaits are stable in the damped model. This means if the system is allowed to flow from initial conditions close to a fixed point, the Poincaré map will tend asymptotically to the point. Thus, to find a fixed point to a given tolerance, we run a forward simulation and average the values of the Poincaré map; the standard deviation in these values provides our estimate of the error.

NUMERICAL STABILITY Since we have yet to provide an analytical result regarding the stability of fixed points of the damped model, we turn to numerical methods to estimate stability. Specifically, we compute the Jacobian of the 4×4 Poincaré Map $\mathcal{P}$,

$$\frac{\partial \mathcal{P}}{\partial(h,\dot{h},\theta,\dot{\theta})} = \begin{bmatrix} \partial_h \mathcal{P}_h & \partial_{\dot{h}} \mathcal{P}_h & \partial_\theta \mathcal{P}_h & \partial_{\dot{\theta}} \mathcal{P}_h \\ \partial_h \mathcal{P}_{\dot{h}} & \partial_{\dot{h}} \mathcal{P}_{\dot{h}} & \partial_\theta \mathcal{P}_{\dot{h}} & \partial_{\dot{\theta}} \mathcal{P}_{\dot{h}} \\ \partial_h \mathcal{P}_\theta & \partial_{\dot{h}} \mathcal{P}_\theta & \partial_\theta \mathcal{P}_\theta & \partial_{\dot{\theta}} \mathcal{P}_\theta \\ \partial_h \mathcal{P}_{\dot{\theta}} & \partial_{\dot{h}} \mathcal{P}_{\dot{\theta}} & \partial_\theta \mathcal{P}_{\dot{\theta}} & \partial_{\dot{\theta}} \mathcal{P}_{\dot{\theta}} \end{bmatrix} \tag{29}$$

PERTURBED TRAJECTORIES As $k_1 \to k_2$, we observe that the system becomes more susceptible to perturbations in that it may begin to switch between equilibrium gaits. For instance, Figure 6 shows two system trajectories, one with $k_1 = 1000$ N/m, $k_2 = 2000$ N/m and the other with k_1 set to 1500 N/m. At the times indicated by the vertical bars, the system was perturbed. Perturbations take the form of instantaneous forces: the first perturbation set $\dot{h}^+ = \dot{h}^- + 0.2$ m/sec, $\dot{\theta}^+ = \dot{\theta}^- - 2$ rad/sec; the second set $\dot{h}^+ = \dot{h}^- - 0.4$ m/sec, $\dot{\theta}^+ = \dot{\theta}^- - 4$ rad/sec. In the first case, the perturbations are rejected, and the system returns to its equilibrium gait. As $k_1 \to k_2$, however, the perturbations switch the system back and forth between the dominant equilibrium gait and the suppressed.

5 RESULTS

Figure 7 shows the model's prediction for how the state of the body at touchdown changes as $k_1 \to k_2$: the angle and angular velocity approach the origin. Ideally, we would generate an identical plot experimentally, however, the state at touchdown is difficult to measure directly with EduBot. Thus we present additional results from the model which are more amenable to experimentation, and compare this data with results from the physical system.

[4]This is intuitively clear since the body in the model will almost certainly roll when, for instance, $k_1 = k_2/2$, but will not roll at all when $k_1 = k_2$, so long as $\theta_0 = \dot{\theta}_0 = 0$ (since in this case the model is equivalent to one with a single spring with spring constant $k = 2k_1 = 2k_2$).

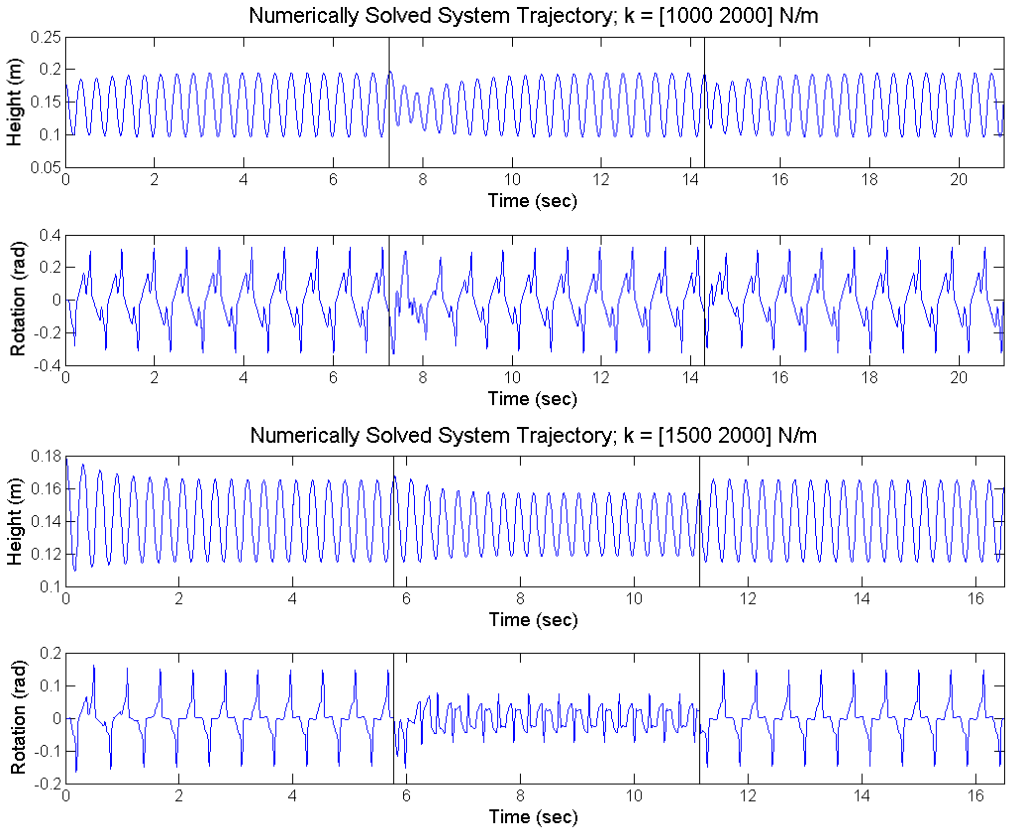

Figure 6: Numerically computed trajectories perturbed at the 20^{th} and 40^{th} touchdown. When $k_1 = 1000$ N/m, the system asymptotically approaches the same equilibrium gait after each perturbation. When $k_1 = 1500$ N/m, the system switches between equilibrium gaits when perturbed.

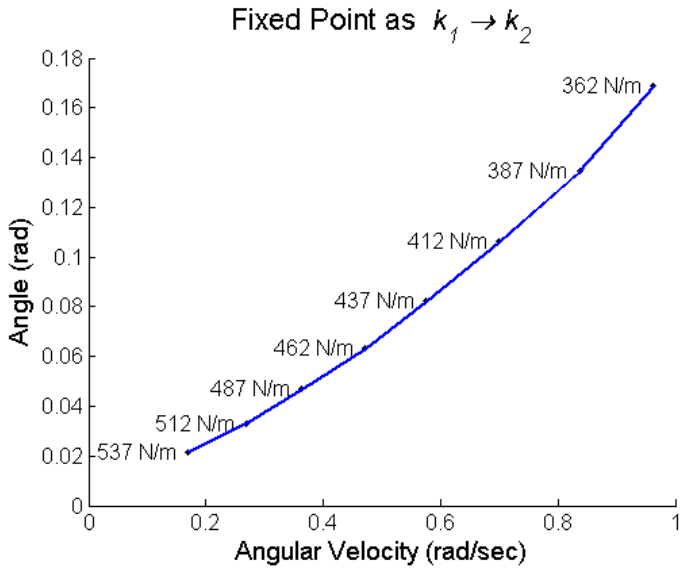

Figure 7: Body state at touchdown as $k_1 \to k_2$.

k_1 (N/m)	Average maximum roll (degrees)	Number of samples
300	4.1 ± 0.4	42
450	2.5 ± 0.6	42
600	1.9 ± 0.5	68

Table 1: As $k_1 \to k_2$, EduBot's roll decreases. Though the decrease is not enormous, it is statistically significant.

5.1 SIMULATION FORCES AND TRAJECTORIES

Figure 8 clearly demonstrates that the average maximum roll at equilibrium decreases as $k_1 \to k_2$.

Figure 9 demonstrates that individual leg ground reaction forces equalize as $k_1 \to k_2$. In the model, if $k_1 = k_2$, then the force patterns would be precisely equal between the legs.

5.2 ROBOT FORCES AND TRAJECTORIES

Table 1 contains the result of averaging the single stride maximum roll EduBot exhibits over a series of experiments. Though the trend is not overwhelming, it does appear that roll decreases as $k_1 \to k_2$.

Figure 10 demonstrates that that the forces exerted on the ground by each leg appear to equalize as $k_1 \to k_2$, however, this data is preliminary.

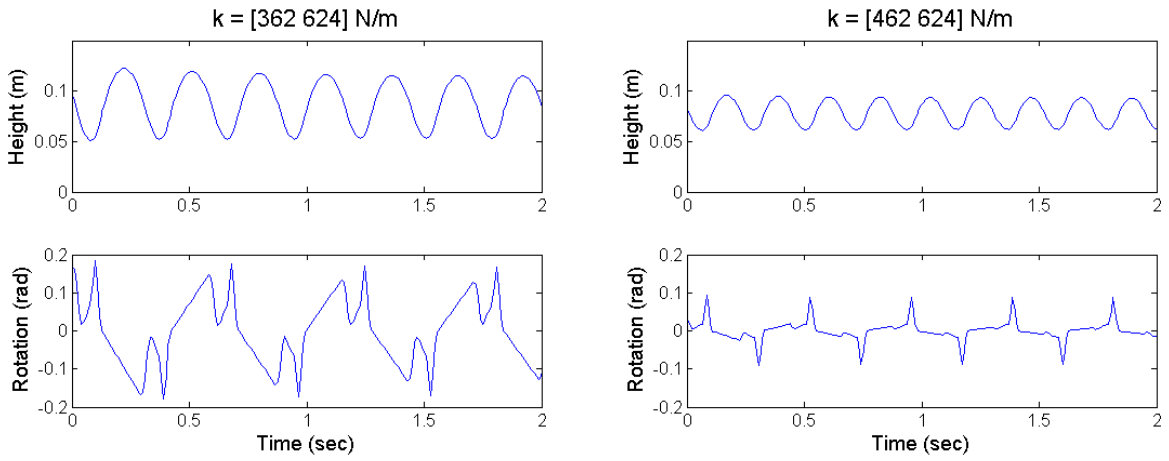

Figure 8: Simulated roll trajectory as $k_1 \to k_2$.

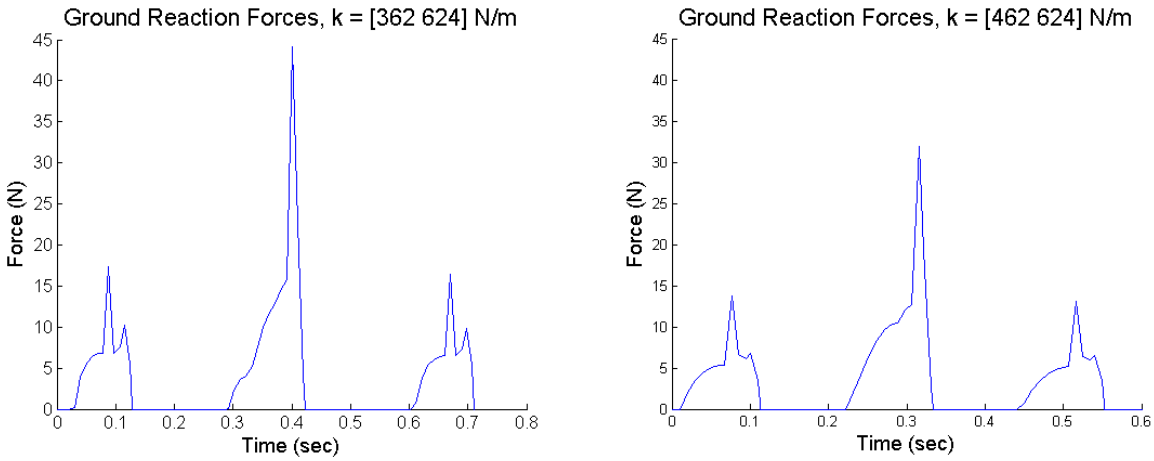

Figure 9: Simulated individual leg forces. We present the data as we would record it experimentally (see Figure 10) for ease of comparison; the first and third ground strikes are identical here.

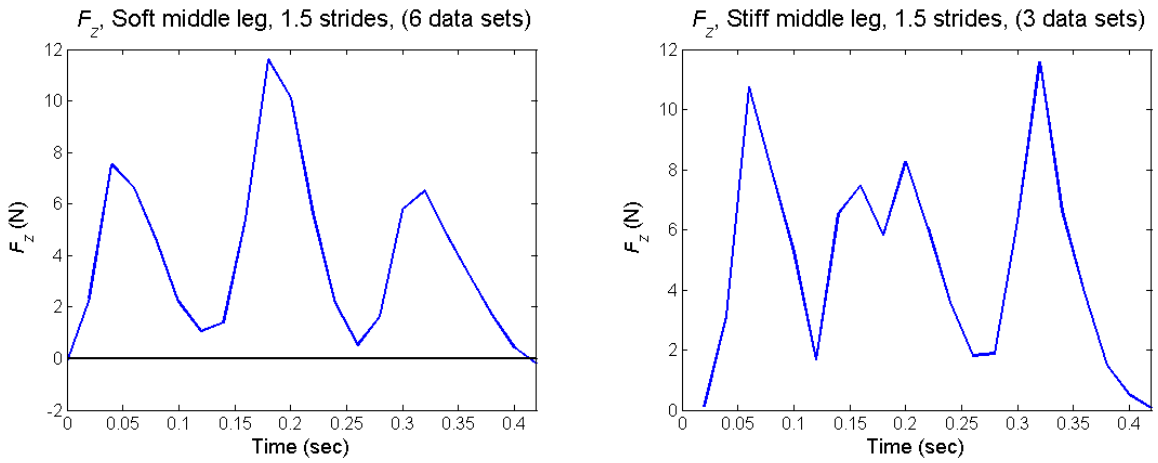

Figure 10: Experimental individual leg forces. From left to right, the three main peaks correspond to the front, middle, and back legs striking the force plate.

6 DISCUSSION

The major contributions of this work are the new analytical model for EduBot's roll and the correspondence between numerical and experimental results that suggest one way to eliminate the robot's roll. This is significant for several reasons. First, despite the success of simple models in describing the sagittal-plane and lateral-plane dynamics of legged locomotion, little work has been put into the analysis of rolling dynamics. Second, since we were able to use this model to predict the effect of a parameter variation in the physical system, we have provided the initial evidence that this model captures something fundamental about the rolling dynamics exhibited by EduBot.

The significance of producing an experimentally valid simple mathematical description of a certain aspect of legged locomotion is subtle. The immediate utility of such a model is that it provides an intuitive framework to think about legged creature's rolling; we are justified in thinking of rolling motion independent from other aspects of a robot's gait, and we understand, qualitatively, the effect of physical parameter variations on roll. In farther-reaching terms, this work could motivate the design of controllers to manipulate rolling in legged robots by providing a plant model, or could inform the design of legged robots themselves by giving insight into the predominant physical processes that lead to rolling.

7 RECOMMENDATIONS

We succeeded in posing the analytical problem of identifying equilibrium gaits in the conservative model using a formal mathematical framework, but we did not make any progress toward actually identifying such fixed points. Future work should therefore be concentrated on producing analytic results in the conservative model. A similar analytical statement can

be constructed for the damped model, and it would be an even more laudable goal to produce analytical results in that case, though we consider this to be a more difficult problem.

We elected to investigate the effect of one parameter variation on roll; this restriction was motivated primarily by the desire to produce an experimentally-verifiable experiment from the model in the time available. There are many more avenues of inquiry that could be taken up in the model, however, like studying the effect of using different energy-addition schemes in the damped model and designing controllers to stabilize the equilibrium gaits of the conservative model. These investigations would likely yield useful insight into how to design and control legged robots.

8 ACKNOWLEDGMENTS

Without the profound support I've received from Dr. Klavins over the past two years, I would not have been able to attend this summer program. Without the significant time and thought invested by Dr. Koditschek, Dr. Clark, and Joel Weingarten, I would not have been nearly so productive or successful this summer as I have been. And without the assistance of Goran Lynch, Dr. Komsuoglu, and the other members of Dr. Koditschek's lab, I would have often been stymied and directionless, not to mention robotless. I would also like to thank the GRASP lab for the use of their motion capture system. Finally, my sincere gratitude goes to Dr. Van der Speigel, the SUNFEST program, and the NSF REU system for organizing and sponsoring this project—I have learned a ridiculous amount this summer.

References

[1] U. Saranli, M. Buehler, and D. Koditschek, Rhex: A simple and highly mobile hexapod robot, *The International Journal of Robotics Research*, 20(7) (2001), 616–631.

[2] S. Bailey, J. Cham, M. Cutkosky, and R. Full, Comparing the locomotion dynamics of a cockroach and a shape deposition manufactured biomimetic hexapod, International Symposium on Experimental Robotics, December 2000.

[3] M. Fend, Whisker-based texture discrimination on a mobile robot, European conference on Advances in Artificial Life, September 2005.

[4] M. Srinivasen, S. Zhang, J. Chahl, G. Stange, and M. Garratt, An overview of insect-inspired guidance for application in ground and airborne platforms, *Proc. Inst. Mech. Eng. Part G J. Aerosp. Eng.*, (2004).

[5] D. Koditschek, R. Altendorfer, and P. Holmes, Stability analysis of legged locomotion by symmetry-factored return maps, *International Journal of Robotics Research*, 23(10-11) (2004), 979–999.

[6] H. Komsuoglu, R. Altendorfer, U. Saranli, D. Koditschek, H. Brown, M. Buehler, M. Moore, D. McMordie, and R. Full, Evidence for spring loaded inverted pendulum running in a hexapod robot, International Symposium on Experimental Robotics, December 2000.

[7] J. Weingarten, G. Lopes, M. Buehler, R. Groff, and D. Koditschek, Automated gait adaptation for legged robots, vol. 3, International Conference on Robotics and Automation, 2004, pp. 2153–2158.

[8] R. Blickhan, The spring-mass model for running and hopping, *Journal of Biomechanics*, 22(11-12) (1989), 1217–1227.

[9] R. Blickhan and R. Full, Similarity in multilegged locomotion: Bouncing like a monopode, *Journal of Computational Physiology*, A(173) (1993), 509–517.

[10] D. Koditschek, R. Altendorfer, and P. Holmes, Stability analysis of a clock-driven rigid-body SLIP model for RHex, *International Journal of Robotics Research*, 23(10-11) (2004), 1001–1012.

[11] T. McGeer, Passive dynamic walking, *International Journal of Robotics Research*, 9(2) (1990), 62–82.

[12] M. Garcia, A. Chatterjee, A. Ruina, and M. Coleman, The simplest walking model: Stability, complexity, and scaling, *Journal of Biomechanical Engineering*, 120(2) (1998), 281–288.

[13] J. Guckenheimer and S. Johnson, Planar hybrid systems, Hybrid Systems II, Springer-Verlag, 1995, pp. 202–225.

[14] J. Guckenheimer and P. Holmes, *Nonlinear oscillations, dynamical systems, and bifurcations of vector fields*, American Mathematical Sciences, no. 42, Springer-Verlag, New York, 2002.

[15] J. Schmitt and P. Holmes, Mechanical models for insect locomotion i. theory, *Biological Cybernetics*, 83 (2000), 501–515.

[16] M. Buehler and D. Koditschek, Analysis of a simplified hopping robot, *International Journal of Robotics Research*, 10(6) (1991), 587–605.

[17] Advanced Mechanical Technology Inc., He6x6 force plate, (2006), http://www.amtiweb.com/index.htm.

[18] Y. Kwon, Force-plate issues, (2006), http://kwon3d.com/theory/grf.html.

[19] The MathWorks Inc., Matlab, (©1994-2006), http://www.mathworks.com/.

A SIMPLE POINCARÉ MAP PROBLEM

When confronted with the task of discovering the long-term behavior of a dynamical system, one approach is to look at the sequence of points where the system intersects a *Poincaré section* [14]. Essentially, a Poincaré section Σ is a surface of codimension 1 embedded in state space. By studying the action of the system on Σ, we can glean information about the system's long-term behavior.

We present here a solution to a simple linear dynamical system problem which utilizes a Poincaré section. This exposition is intended to motivate the analysis we later set up to apply to the conservative model for EduBot's rolling.

DEFINE

$$x = \begin{bmatrix} x_1 \\ x_2 \end{bmatrix}, \quad \dot{x} = (\sigma I + \omega J)x, \quad I = \begin{bmatrix} 1 & 0 \\ 0 & 1 \end{bmatrix}, \quad J = \begin{bmatrix} 0 & 1 \\ -1 & 0 \end{bmatrix},$$

$$q = \begin{bmatrix} \rho \\ \theta \end{bmatrix} = \begin{bmatrix} \sqrt{x_1^2 + x_2^2} \\ tan^{-1}(x_1, x_2) \end{bmatrix}, \quad \Theta = \{(\rho, \theta) \in \mathbb{R} \times \mathbb{S}^1 \mid \theta = 0\}.$$

(We adopt the convention that $\theta = tan^{-1}(y, x)$ implies $x = \cos\theta$, $y = \sin\theta$.)

Define a *Poincaré map* $\mathcal{P} : \Theta \to \Theta$ in the following way: if $x(t, x_0)$ solves the differential equation[5] and $\Theta(x(\tau_k)) = 0$ with $\rho(x(\tau_k)) = \rho_{\tau_k}$, then $\mathcal{P}(\rho_{\tau_k}) = \rho_{\tau_{k+1}}$, where $\tau_{k+1} = \min_{t>\tau_k}\{\theta(x(t)) = 0\}$.

So, intuitively, if x_1 lies along the y-axis and x_2 along the x-axis, Θ is the set of points where a solution to the differential equation crosses the positive x-axis, and $\mathcal{P}$ maps such points onto the next such point in (temporal) order of occurrence.

FIND An explicit formula for $\rho_{\tau_{k+1}} = \mathcal{P}(\rho_{\tau_k})$.

GENERAL SOLUTION The general solution to the differential equation is given by

$$x(t, x_0) = \begin{bmatrix} x_1(t) \\ x_2(t) \end{bmatrix} = \begin{bmatrix} e^{\sigma t}(\overline{x}_1 \cos(\omega t) + \overline{x}_2 \sin(\omega t)) \\ e^{\sigma t}(-\overline{x}_1 \sin(\omega t) + \overline{x}_2 \cos(\omega t)) \end{bmatrix}, \quad x_0 = \begin{bmatrix} \overline{x}_1 \\ \overline{x}_2 \end{bmatrix}. \tag{30}$$

STRUCTURE OF Θ Given $\theta = tan^{-1}(x_1, x_2)$, it is clear that $\theta = 0 \iff x_1 = 0,\ x_2 > 0$. But

$$x_1(t) = 0 \iff \overline{x}_2 \sin(\omega t) = -\overline{x}_1 \cos(\omega t) \iff \tan(\omega t) = -\frac{\overline{x}_1}{\overline{x}_2}, \tag{31}$$

$$x_2(t) > 0 \iff -\overline{x}_1 \sin(\omega t) + \overline{x}_2 \cos(\omega t) > 0. \tag{32}$$

[5] In this case, we find it convenient to drop the x_0 argument and simply call the solution $x(t)$.

The condition in eq. 31 gives two possible choices for ωt which lie in opposing quadrants (i.e. I and III or II and IV); the condition in eq. 32, when taken with the result from eq. 31, selects one of these two choices (the choice where $\sin(\omega t) < 0$).

Note that since $\sin(\omega t)$ and $\cos(\omega t)$ are $\frac{2\pi}{\omega}$-periodic, a solution τ_0 determined from eqs. 31 & 32 gives rise to an entire sequence of solutions of the form $\{\tau_k = \tau_0 + \frac{2\pi}{\omega}k \mid k \in \mathbb{N}\}$. Note also that consecutive terms in this sequence provide the proper temporal ordering on events in Θ, by which we mean $\tau_{k+1} = \min_{t>\tau_k}\{\theta(x(t)) = 0\}$.

FINDING $\mathcal{P}(\rho_{\tau_k})$ We are nearly finished. We have the sequence of times corresponding to points in Θ, so all that remains is to evaluate ρ at the (x_1, x_2) coordinates corresponding to those times.

First, note that an event in Θ requires $x_1 = 0$, so $\rho_{\tau_k} = x_2(\tau_k)$. Next, note that by construction $\tan(\omega\tau_k) = -\frac{\overline{x}_1}{\overline{x}_2}$, $\sin(\omega\tau_k) < 0$, so

$$\sin(\omega\tau_k) = \frac{-\overline{x}_1}{\sqrt{\overline{x}_1^2 + \overline{x}_2^2}},\ cos(\omega\tau_k) = \frac{\overline{x}_2}{\sqrt{\overline{x}_1^2 + \overline{x}_2^2}}. \tag{33}$$

So by combining eq. 33 with eq. 30, we have

$$\rho_{\tau_k} = x_2(\tau_k) = e^{\sigma\tau_k}\left(\frac{\overline{x}_1^2 + \overline{x}_2^2}{\sqrt{\overline{x}_1^2 + \overline{x}_2^2}}\right). \tag{34}$$

Now, recognizing that the next event occurs at time $\tau_{k+1} = \tau_k + \frac{2\pi}{\omega}$,

$$\rho_{\tau_{k+1}} = \mathcal{P}(\rho_{\tau_k}) = e^{\sigma(\tau_k + \frac{2\pi}{\omega})}\left(\frac{\overline{x}_1^2 + \overline{x}_2^2}{\sqrt{\overline{x}_1^2 + \overline{x}_2^2}}\right) = e^{\frac{2\pi\sigma}{\omega}}\rho_{\tau_k}, \tag{35}$$

and, more generally,

$$\rho_{\tau_{k+n}} = \mathcal{P} \circ \cdots \circ \mathcal{P}(\rho_{\tau_k}) = \mathcal{P}^n(\rho_{\tau_k}) = e^{\frac{2\pi\sigma}{\omega}n}\rho_{\tau_k}. \tag{36}$$

SYSTEM BEHAVIOR Assuming at least one of the initial conditions is nonzero, choices of σ and ω determine the qualitative behavior of the system.

If $\sigma = 0$, the system moves in a circle. If $\sigma < 0$, the system spirals toward the origin. If $\sigma > 0$, the system spirals toward infinity. Note that these qualitative statements are reflected in eq. 36, and given precise analytical meaning—*this is the primary utility of such a solution.*

If $\omega = 0$, the system moves along a ray: toward infinity, toward the origin, or remaining stationary, depending on the choice of σ. In this case, the conclusion that the system's dynamics are $\frac{2\pi}{\omega}$-periodic is invalid, and either $\Theta \equiv \emptyset$ or $\Theta \subset \mathbb{R}$, depending on the choice of initial conditions.

B FORCE PLATE

We measure the *ground reaction forces* for EduBot using a commercially-available force plate [17]. The force plate uses Hall Effect sensors to measure the net force $\mathbf{F} = (F_x, F_y, F_z)^T$ and moment $\mathbf{M} = (M_x, M_y, M_z)^T$ applied to the *center of pressure* of the surface.

The plate either outputs analog signals which can be combined to compute $\mathbf{F}$ and $\mathbf{M}$ or a digital signal which can be used with proprietary software to save the net force and moment to an ASCII text file at 12 bit resolution and up to 200 Hz.

Given $\mathbf{F}$ and $\mathbf{M}$, we wish to find the net z-axis torque T_z applied to the plate. From [18], we know that

$$\mathbf{M} = (x - a, y - b, \tau - c) \times \mathbf{F} + (0, 0, T_z), \tag{37}$$

where (a, b, c) is the actual origin for the force plate (given by the manufacturer's *calibration matrix*), τ is the thickness of whatever padding is added to the surface of the force plate, and T_z is the net torque applied to the plate about the z-axis.

Writing this equation in matrix form, we have

$$\mathbf{M} = \begin{bmatrix} M_x \\ M_y \\ M_z \end{bmatrix} = \begin{bmatrix} 0 & -(\tau - c) & y - b \\ \tau - c & 0 & -(x - a) \\ -(y - b) & (x - a) & 0 \end{bmatrix} \begin{bmatrix} F_x \\ F_y \\ F_z \end{bmatrix} + \begin{bmatrix} 0 \\ 0 \\ T_z \end{bmatrix}, \tag{38}$$

so we arrive at

$$x = -\frac{M_y + (c - \tau)F_x}{F_z} + a, \tag{39}$$

$$y = \frac{M_x - (c - \tau)F_y}{F_z} + b, \tag{40}$$

$$z = \tau, \tag{41}$$

$$T_z = M_z - (x - a)F_y + (y - b)F_x. \tag{42}$$

So now given $\mathbf{F}$ and $\mathbf{M}$ from the force plate, we can extract the *center of pressure* and the net force and torque exerted by the robot.

C NUMERICAL METHODS

We performed numerical simulations in MATLAB [19] using the `ode45` numerical solver with `RelTol` $= 1 \times 10^{-8}$, `AbsTol` $= 1 \times 10^{-6}$. We computed equilibria in the conservative model to within 1% in all coordinates unless otherwise specified. Vector field plots contain 30 subdivisions in each coordinate; trajectories that fail to produce a touchdown event are omitted. We used `ode45`'s built-in *event function* feature to implement the hybrid dynamics of the model.

D TRAJECTORY MEASUREMENTS

Robot trajectories were recorded using a motion-capture system. The system treats EduBot like a rigid body in $\mathbb{R}^3$, recording the robot's position and three-axis rotation at roughly 120 Hz with sub-millimeter accuracy. Occasionally the motion capture system loses track of the robot for one to five samples; in this case, we interpolate linearly across the lost samples. We then apply a 5-sample median filter to smooth jump discontinuities in the data that appear to be introduced by noise.